International Journal of Biological Macromolecules 235 (2023) 123777

Contents lists available at ScienceDirect

International Journal of Biological Macromolecules

journal homepage: www.elsevier.com/locate/ijbiomac

Injectable hybrid hydrogels physically crosslinked based on carrageenan and green graphene for tissue repair

Danny Moncada [a], Maite Rico [a], Belén Montero [a], Saddys Rodríguez-Llamazares [b], Sandra Feijoo-Bandín [c], Oreste Gualillo [d], Francisca Lago [c], Alana Aragón-Herrera [c], Horacio Salavagione [e], Natalia Pettinelli [b], Rebeca Bouza [a,*], Yousof Farrag [d]

[a] Universidade da Coruña, Grupo de Polímeros, Departamento de Física y Ciencias de la Tierra, Escuela Politécnica de Ingeniería de Ferrol, C/ Mendizábal, s/n, 15403 Ferrol, A Coruña, Spain
[b] Centro de Investigación de Polímeros Avanzados, Edificio Laboratorio CIPA, Av. Collao 1202, Concepción, Chile
[c] IDIS (Instituto de Investigación Sanitaria de Santiago), Molecular and Cellular Cardiology Group, Santiago University Clinical Hospital, Building C, Travesía da Choupana S/N, 15706 Santiago de Compostela, Spain
[d] IDIS (Instituto de Investigación Sanitaria de Santiago), NEIRID Group (Neuroendocrine Interactions in Rheumatology and Inflammatory Diseases), Santiago University Clinical Hospital, Building C, Travesía da Choupana S/N, 15706 Santiago de Compostela, Spain
[e] Departamento de Física de Polímeros, Elastómeros y Aplicaciones Energéticas, Instituto de Ciencia y Tecnología de Polímeros (ICTP-CSIC), C/ Juan de la Cierva 3, 28006 Madrid, Spain

ARTICLE INFO

Keywords:
Injectable hydrogels
Carrageenan
Graphene

ABSTRACT

Injectable and biocompatible novel hybrid hydrogels based on physically crosslinked natural biopolymers and green graphene for potential use in tissue engineering are reported. Kappa and iota carrageenan, locust bean gum and gelatin are used as biopolymeric matrix. The effect of green graphene content on the swelling behavior, mechanical properties and biocompatibility of the hybrid hydrogels is investigated. The hybrid hydrogels present a porous network with three-dimensionally interconnected microstructures, with lower pore size than that of the hydrogel without graphene. The addition of graphene into the biopolymeric network improves the stability and the mechanical properties of the hydrogels in phosphate buffer saline solution at 37 °C without noticeable change in the injectability. The mechanical properties of the hybrid hydrogels were enhanced by varying the dosage of graphene between 0.025 and 0.075 w/v%. In this range, the hybrid hydrogels preserve their integrity during mechanical test and recover the initial shape after removing the applied stress. Meanwhile, hybrid hydrogels with graphene content of up to 0.05 w/v% exhibit good biocompatibility for 3T3-L1 fibroblasts; the cells proliferate inside the gel structure and show higher spreading after 48 h. These injectable hybrid hydrogels with graphene have promising future as materials for tissue repair.

1. Introduction

Hydrogels have become an important focus of study in pharmaceutical and biomedical research due to their attractive characteristics and close resemblance to the extracellular matrix (ECM) [1], e.g., acting as physical barriers, fluid absorbents and their biocompatibility and ability to provide scaffolding [2,3]. In the last decades, highly variable hydrogels with a multitude of functions have been developed. Hydrogels are classified according to several factors: the origin of the polymeric network (natural, synthetic or hybrid) [4–8], the preparation method [9,10] and the type of crosslinking (physical or chemical) [11–13]. Hydrogels have wide range of applications that includes tissue engineering, wound healing, and injury treatment [14], as a vehicle for localized and controlled delivery of cells, pharmacological molecules, and growth factors [15–19]. Injectable hydrogels can be administrated through minimally invasive procedure, thus decreasing recovery times and infection risks [20,21].

Wide variety of hydrophilic natural and synthetic materials, including hyaluronic acid, chitosan, gelatin, alginate, silk fibroin, carrageenan, poly(ethylene glycol) (PEG), and poly(lactic-co-glycolic acid) (PLGA) [22–24] have been investigated as injectable hydrogels. Carrageenans are hydrophilic and anionic linear sulfated galactan

* Corresponding author.
E-mail address: rebeca.bouza@udc.es (R. Bouza).

https://doi.org/10.1016/j.ijbiomac.2023.123777
Received 18 November 2022; Received in revised form 14 February 2023; Accepted 16 February 2023
Available online 20 February 2023
0141-8130/© 2023 The Authors. Published by Elsevier B.V. This is an open access article under the CC BY license (http://creativecommons.org/licenses/by/4.0/).

polymers extracted from red algae. There are three main types of carrageenans, kappa carrageenan (κC), iota carrageenan (ιC) and lambda carrageenan (λC), which differ in their structure, molecular weight and the amount of sulfate groups present [25]. These structural differences provide specific characteristics in terms of solubility, ability to interact with metal ions, and gelation behavior [26]. Both κC and ιC are formed by alternating polymeric chains of D-galactose and 3,6-anhydro-D-galactose (3,6 - AG) linked through α-1,3 and β-1,4 glycosidic bonds [27,28], while λ-carrageenan is only composed of D - galactose units. Gels formed by κC in the presence of potassium ions (K^{+}) are strong and rigid, while gels formed by ιC in the presence of calcium ions (Ca^{+2}) are softer and more elastic. As for λC, the high degree of sulfation, the position occupied by the sulfate groups within the chemical structure and the absence of 3,6-GA, prevent its crosslinking and gelation [29]. However, some studies have described its possible gelation through trivalent ions such as iron ions, which allow favourable interactions between λ-carrageenan chains [30,31]. Hydrogels formed with this natural polymer possess high water-holding capacity, modifiable gelling properties, thermo-reversibility, low toxicity, and high water-holding capacity [32].

In addition to the sulfate groups, other components were identified in the chemical structure of carrageenans, such as xylose, glucose, uronic acids, methyl esters and/or pyruvate groups [33–35] that allow modifying certain gel characteristics. Another way to change and improve the properties of a gel is by mixing with other compounds such as gelatin, cellulose, locust bean gum, etc. [2,3,36].

Graphene is a two-dimensional (2D) material that is composed of a monolayer of sp^2-bonded carbon atoms arranged in a hexagonal lattice, forming strong covalent bonds between adjacent carbons. Depending on the synthetic procedure, the characteristics of the graphene layers in terms of different aspect ratios, type and number of functional groups attached to the structure, and the ratio of sp^2 to sp^3 carbon atoms can be controlled [37,38]. The superior properties of graphene, such as tensile strength, Young's modulus, thermal and electrical conductivity allow it to improve the properties of other materials, such as carrageenan, improving its mechanical robustness by acting as a structural support. There is scarce information on how pristine graphene affects medical trials and research so far has focused on the use of graphene derivates. The most used graphene-like structures are graphene oxide (GO), reduced graphene oxide (rGO), and carbon nanotubes (CNTs) [39,40] rich in oxygen functional groups such as hydroxyl (-OH), carboxylic acids (-COO), carbonyl (C-O) and epoxide groups [41]. In contrast to oxidized graphene, the structure of pristine graphene is not greatly affected by the preparation method due to its chemical structure, free or low number of functional groups. These functional groups provide new features allowing covalent and non-covalent bonds. However, the results show that the interaction between GO nanosheets and the hydrogel matrix was slightly weak [42,43].

Recently, injectable nanohybrids of carrageenan with graphene ant its derivatives have been developed, which has opened a path in the search for new possibilities of applications of these materials. Graphene and its derivatives, such as GO and rGO, are attracting increasing attention in biomedical and pharmacological research due to their biocompatibility along with outstanding electrical, mechanical, and thermal properties [43–45]. Some evidence of this is the use of a κC-grafted graphene oxide-based nanocarrier conjugated with biotin for controlled and targeted drug delivery in cancer treatment [46], κC with dopamine-functionalized graphene oxide for tissue engineering [47] and carrageenan-acrylic acid-graphene-hydroxyapatite as scaffolds for bone regeneration [48,49].

Using more than one component to form the biopolymeric network of the hydrogel helps in tuning the final properties towards the needs of the desired application. The carrageenans present a thixotropic behavior that makes it appropriate to form injectable matrices for the transport of cells or some active principle [50]. While kappa carrageenan offers the strength and rigidity required for a stable hydrogel, iota carrageenan is known for producing softer hydrogels that can offers the required ductility for an injectable product. In addition, the mechanical performance of a hydrogel of a mixture of these carrageenans was reported to better than the sum of the corresponding individual gels [50]. As for locust bean gum (neutral polysaccharide), it does not form gels under normal conditions, but it can act synergistically with kappa carrageenan allowing the formation of elastic and strong gels [51] due to its ability to interact with the surface groups of carrageenan through hydrogen bridge bonds. Gelatin is known to improve cells adhesion and proliferation on polymeric matrices. Besides, it can form thermos-reversible gels with kappa carrageenan, capable of having a synergetic effect [52], increasing mechanical strength, improving flexibility [2].

In the particular case of graphene/carrageenan composites, the design of a hybrid hydrogel that combines the best characteristics of both components should consider the required levels of mechanical properties such as recovery efficiency, toughness, elasticity, and fatigue resistance, for possible applications. The objective of this study was the development of new injectable hybrid hydrogels using physically crosslinked natural biopolymers and graphene or tissue repair. Kappa and iota carrageenan, locust bean gum, gelatin and green graphene were used for its preparation. The properties of graphene and the physical interactions, surface morphologies, swelling behavior, biocompatibility and mechanical properties of the prepared hydrogels were evaluated to assess their potential for tissue repair.

2. Materials and methods

2.1. Materials

The kappa carrageenan (κC) (MW ~ 500 kDa), iota carrageenan (ιC) (MW = 300 kDa) and locust bean gum (LB) (viscosity 3500 cps, 25 °C) were kindly gifted by Ceamsa, Spain. Gelatin was obtained from BD, USA. Potassium chloride and calcium chloride were of analytical grade and purchased from Scharlau, Spain. The graphene powder 99 % (GR) was kindly supplied by GreenTech, Spain. The sustainable and ecological manufacturing process of this graphene allows reducing production costs to obtain high quality graphene powder. All chemicals were used without further purification. The water used in the preparation and the dialysis was purified in a Milli-Q ultrapure system (Millipore, France).

2.2. Preparation and characterization of the graphene dispersions

2.2.1. Preparation of the graphene dispersions

Solutions of ιC (1 and 2 % w/v), gelatin (1 % w/v), and κC (1 % w/v) in water were prepared by stirring and heating at 70 °C, 50 °C, and 80 °C respectively. The graphene powder was added to each of these solutions at a concentration of 0.5 % w/v and then kept under constant stirring for approximately 15 min. Subsequently, ultrasonication was applied for 10 min using an ultrasonic processor SONOPULS HD 3200 (Bandelin electronics, Germany) equipped with a titanium microtip of 7 mm diameter. The applied ultrasonic power was up to 200 W and the processing frequency was 20 kHz. The resulted suspension was centrifuged for 3 min at 5000 rpm.

2.2.2. Raman spectroscopy

The Raman spectra measurements were performed using a Renishaw InVia-Reflex Raman system (Renishaw plc, Wotton-under-Edge, UK), which employed a gratin spectrometer with a Peltier-cooler CCD detector coupled to a confocal microscope. Raman scattering was excited with an argon ion laser (λ = 785 nm), at 1 % of power and 20 scans were accumulated per sample using a 100× microscope objective (NA = 0.85). Spectra were recorded in the range between 100 and 3200 cm^{-1} from several positions. All spectral data were processed with Renishaw WiRE 5.0 software. The analysis was performed on the graphene powder as well as the graphene dispersion in 2 % ιC solution from the spun sample of ιC + GR from which a small drop was deposited on a silica

plate.

2.2.3. UV- visible spectroscopy

To evaluate the dispersion of graphene in different solutions, the electronic spectra of diluted graphene dispersions (1/10) were measured in a Lambda 35 UV/VIS Spectrometer, Perkin Elmer (Norwalk, CT, USA) in the region of 400 nm to 800 nm at a scan rate of 240 nm min^{-1}. The results were analyzed using uv.winLab software.

2.3. Hydrogels preparation

The solutions of ιC (1 and 2 % w/v), gelatin (1 % w/v), κC (1 % w/v) and the graphene suspension in ιC solution were prepared as described before [53]. The graphene injectable hydrogels (IH + GR) were prepared by mixing 6 mL of κC/LB solution, 1 mL of gelatin solution, and different amounts of ιC/GR dispersion and the ιC solution reaching final volume of 10 mL. The final graphene concentrations in the hydrogel formulations and the corresponding sample names are summarized in Table 1. The mixtures were magnetically stirred at 55 °C then, 300 μL of 0.5 M KCl and 150 μL of 0.5 M $CaCl_2$ were added to promote gelation. The mixtures were left at room temperature for approximately 1 h for complete gelling. A control hydrogel (IH) was prepared replacing the ιC/GR dispersion with ιC solution.

2.4. Mechanical properties

The mechanical properties of the hydrogels including the compressive modulus and the compressive strain at break point were evaluated using an Instron Universal Testing Machine 5565 (Instron, England) with a 100 N load cell and a crosshead speed of 2 mm min^{-1}. Cylindrical hydrogel samples with a diameter of 25 mm and a height of 10 mm were used for the compression tests. Compressive modulus was defined as the slope of the linear region of the strain/stress curves, corresponding to 5–15 % strain. Data of the compressive strain correspond to the strain at the yield point. The results were reported as the mean ± standard error of at least seven specimens.

2.5. Injectability

To evaluate the smoothness and injectability visually, the hydrogels were loaded into 10 mL syringes with a 18G needle and injected by hand. The IH was spiked with methylene blue to improve visualization.

2.6. Swelling behavior

The swelling behavior of the lyophilized hydrogels was determined from freeze-dried hydrogels immersed in phosphate buffer saline (PBS) solution at 37 °C. The swollen hydrogels were weighed daily after removing the water until equilibrium or degradation was reached. Surface water was absorbed by filter paper before weighing. The equilibrium swelling ratio (SR) [54] was calculated by Eq. (1).

$$SR = \left[\frac{W_s - W_i}{W_i}\right] \quad (1)$$

Table 1
Final concentration of graphene in each hydrogel.

Sample code	GR final concentration w/v %
IH	0
IH + GR-0.01	0.01
IH + GR-0.02	0.02
IH + GR-0.025	0.025
IH + GR-0.05	0.05
IH + GR-0.075	0.075
IH + GR-0.1	0.1
IH + GR-0.15	0.15

where W_S is the weight of the swollen hydrogel and W_i is the initial weight of the lyophilized hydrogel.

2.7. Scanning electron microscopy (SEM)

To evaluate the surface morphological structures, the freeze-dried hydrogels were sputter- coated with iridium using a Cressington 208HR high-resolution sputter coating (Cressington Scientific Instrument, UK). The surface morphologies were observed with a JSM 7200F field emission scanning electron microscope (Jeol, USA) at an accelerating voltage of 10 kV and 15 kV.

2.8. Cell assays

2.8.1. Cell cultures

3T3-L1 murine fibroblasts, purchased from American Type Culture Collection (ATCC) USA, were cultured in high glucose (4.5 g L^{-1}) Dulbecco's modified eagle medium (DMEM) (Lonza Group Ltd, Switzerland) supplemented with 10 % heat-inactivated fetal bovine serum (FBS) (Merck KGaA, Germany), 2 % penicillin/streptomycin antibiotics and 2 % L glutamine (Sigma-Aldrich, USA) at 37 °C and 5 % CO_2.

2.8.2. Confocal laser microscopy

Hydrogels were prepared in a thin monolayer on 35 mm dishes with glass bottom (Ibidi GmbH, DE) and left under ultraviolet light for 2 h. 3T3-L1 fibroblasts were seeded on the hydrogel and then cultured for 24 h and 48 h. Cells were simultaneously stained with 7 μM propidium iodide (PI) (Merck KGaA, DE) and with 2.5 μM calcein-AM (Thermo Fisher Scientific Inc., US) to discriminate between dead (red staining) and live cells (green staining), respectively. Images were taken using the confocal microscope Leica TCS SP8 MP (Leica Microsystems AG, Wetzlar, Germany). Stacking analysis was recorded at each time point using 30 cross- sections. Image-J software (1.53 s) was used for cell counting from at least 4 images of 1 mm^2 area, taken from different positions of each hydrogel sample.

2.8.3. Statistical analysis

Data of the mechanical properties was analyzed using one-way analysis of variance (ANOVA) test. The significance between groups of the results of compressive moduli and compressive strain at break point were checked by Tukey post-hoc and Kruskal-Wallis test, respectively. Data of the cell assay are reported as the mean ± standard error of the mean of at least three independent experiments. Statistical analyses were performed with GraphPad Prism 9.3.1 software (GraphPad Software, USA). ANOVA test followed by Bonferroni's multiple comparison test was performed to compare the data. A P value <0.05 was considered as significant.

3. Results and discussion

3.1. Optimization of graphene dispersion

3.1.1. Raman spectroscopy

Raman spectroscopy was used to distinguish the ordered and disordered crystalline structures of carbon in the graphene powder where three characteristic bands can be distinguished, the D, G, and the 2D bands (Fig. 1). The G band (1582 cm^{-1}) corresponds to the vibration of the sp^2 carbon atoms in the two-dimensional hexagonal network. This position is the same for both graphite and graphene [39,55]. The 2D band shape and relative intensity (2615 cm^{-1}) allows us to assess thickness of graphene. In this case, the 2D/G intensity ratio suggests good exfoliation producing few-layer graphene. It is also possible to observe the disorder induced D band with high intensity at (1309 cm^{-1}) as well as the splitting of the G band (1582 cm^{-1} and 1605 cm^{-1}, the latter corresponding to edge defects) indicating disorder and defects in

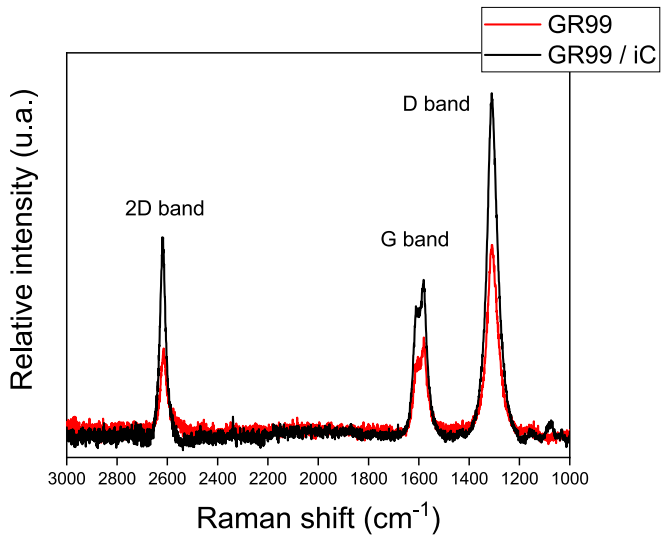

Fig. 1. Raman spectra of graphene powder and the graphene (0.5 % w/v) dispersed in ιC (2 % w/v).

the graphene nanosheets [56]. The intensity ratio between the D and G bands (I_D/I_G) was calculated at 2.1 which is indicates the presence of defects or imperfections in the graphene sheets, in good agreement with previous reports for graphene derivatives with similar D/G ratios [57].

The Raman spectra of the graphene (0.5 % w/v) suspension in ιC (2 % w/v) showed similar peaks as the graphene powder, suggesting that no significant changes occur under the dispersion procedure (Fig. 1).

3.1.2. UV–visible spectroscopy

The UV–Vis spectroscopy was used to determine the most adequate polymeric solution for the suspension of graphene. The UV–vis spectra of graphene lack of absorbance peaks in the visible region [58]. Nevertheless, an upward baseline shift within this region is normally observed due to the light scattering caused by the dispersed nanoparticles [59]. Therefore, the greater the baseline shift, the greater the concentration of dispersed particles in solution. The dispersion of graphene was evaluated by UV–Vis spectroscopy in 10-fold diluted 0.5 % w/v graphene suspensions in 1 % w/v gelatin, ιC, and κC solutions, in addition to 2 % w/v ιC solution. Fig. 2A shows the absorbance of the different solutions used for graphene dispersion without applying ultrasound. The graphene suspension in gelatin showed the lowest baseline shift, followed by ιC (1 % w/v), κC, being the highest ιC solution at 2 % w/v. The application of ultrasound for 5 min increased the baseline shift for the graphene suspension in 2 % w/v ιC. Increasing the ultrasonication time to 10 min further increases the shifting, which indicate improved graphene dispersion (Fig. 2B).

With these results the dispersion of graphene in ιC/GR 2 % was selected for hydrogel preparation. Samples prepared with this dispersion and listed in Table 1 will be discussed hereafter.

3.2. Hydrogel characterization

3.2.1. Mechanical properties

The mechanical properties of the hydrogels listed in Table 1 were measured by applying compression stress–strain tests. The effect of the incorporation of graphene on the compressive modulus and the compressive strain at break point of the hydrogels is shown in Fig. 3.

The compressive modulus of physically crosslinked hydrogel increased gradually with the loading of green graphene (0.025 to 0.075 w/v%) from 50 ± 5 kPa (at IH) to 75 ± 4 kPa (at HI + GR-0.075) (Fig. 3A). Therefore, the incorporation of graphene significantly improved the compression modulus by >50 % compared to the IH hydrogel. These results indicate strong interfacial interaction between the graphene and the hydrogel components at relatively low graphene concentrations. At graphene concentrations higher than 0.075 w/v%, the modulus decreased to values similar to IH hydrogel. The drop of modulus could be attributed to the agglomeration of graphene laminates, which are prone to adhere together, and form agglomerates due to its high surface area. These graphene agglomerates act as stress-concentration points and cannot mitigate the proper stress transfer from graphene (high elastic domain) to the highly viscoelastic polysaccharide gel matrix, [60]. The compressive moduli of the hybrid hydrogels in this study were found to be much greater than those reported for polysaccharide hydrogels reinforced with graphene, including methacrylate- kappa-carrageenan-dopamine functionalized with 1 % of graphene oxide (40 kPa) [47], chitosan-based hydrogel nanocomposites with 0.8 wt% of graphene oxide (0.104 kPa) [61], and chitosan/β-glycerophosphate with 0.04 wt% of graphene oxide (11.6 kPa) [62].

The compressive strain at break point did not show a clear trend with the graphene concentration (Fig. 3B). A significant increase is observed for the sample with the lowest loading, followed by a slight diminution at intermediate loadings until an important drop for the samples with the highest graphene loading. Nevertheless, it is worth mentioning that the IH completely collapsed under 80 % of compressive strain (Fig. 3C), while hybrid hydrogels with 0.025 and 0.075 w/v % of graphene were able to preserve their integrity under the same strain and to fully recover the original shape after releasing the applied stress (Fig. 3D). A hypothetical reason of complete recovery hybrid hydrogel after uniaxial

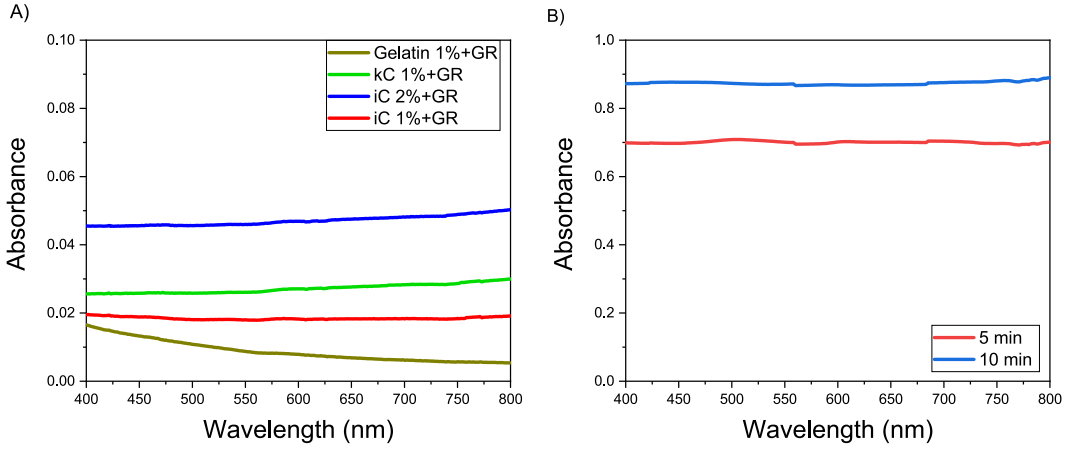

Fig. 2. Absorbance of graphene dispersed in different solutions: A) gelatin (1 % w/v), κC, (1 % w/v) and ιC (1 % and 2 % w/v). B) The spectra of the graphene suspension in ιC (2 %) applying different ultrasonication times (5 min and 10 min).

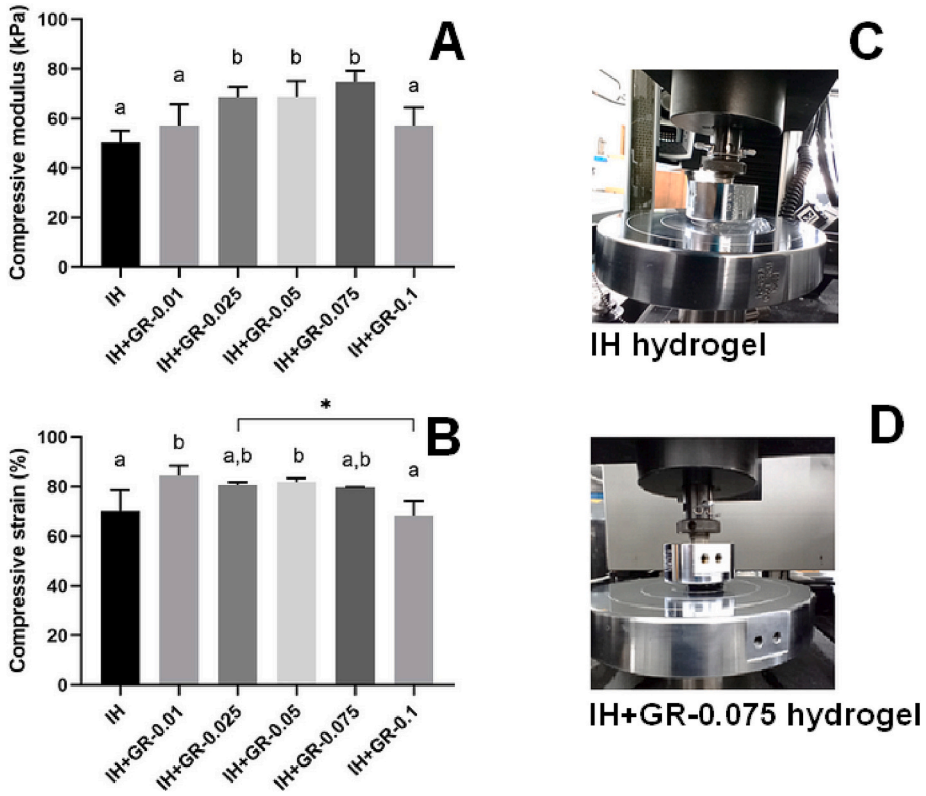

Fig. 3. Effect of green graphene content on the compressive modulus (A) and compressive strain at break point of hydrogels (B). Error bars show standard deviation; sample size n > 7. Values with different letters (a and b) or * in the columns are statistically different at P < 0.05 by Kruskal-Wallis test. Compression test photographs of hydrogels IH (C) and IH + GR-0.075 (D) under 70 % of compressive deformation.

compression resides on physical interaction of polymer chains onto graphene, which provides another physical secondary bonding. This additional physical interaction could be the cause for recovering its mechanical property in a short time [63].

3.2.2. Injectability

Pettinelli et al. have reported on a hydrogel with similar polymeric components as the reported in this study, which presents shear thinning properties. Thus, the hydrogel displays reduced viscosity upon applying shear force. This property is of paramount importance in viscoelastic hydrogels intended for injection as they can pass the syringe needle relatively easy and then recover their original mechanical properties after injection [2]. The injectability of the hydrogels was visually assessed by applying pressure with a syringe needle (Fig. 4). Upon the application of a shear force, all hydrogels flowed continuously through the syringe needle (Fig. 4). The presence of dispersed graphene sheets does not seem to affect the injectability of the hydrogels, thus these hydrogels can be envisaged as potential candidates for applications requiring localized injectability.

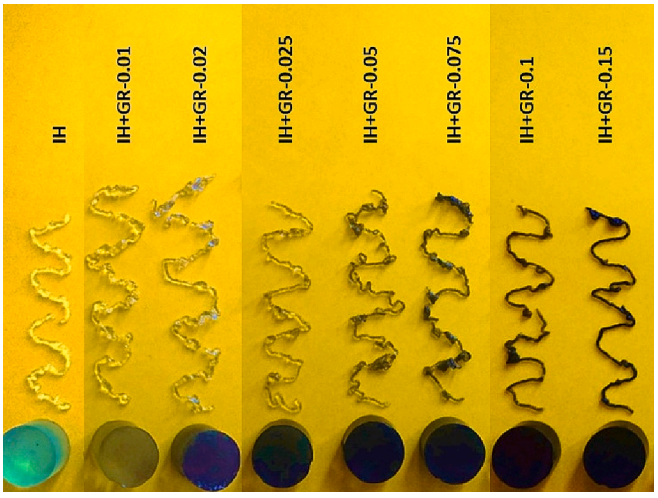

Fig. 4. Injectability by hand of hydrogels.

3.2.3. Swelling behavior

The water absorption capacity within the porous hydrogel structure is one of the main useful characteristics of hydrogels for tissue engineering. This allows the diffusion and delivery of nutrients, active molecules such as drugs and growth factors, in addition to being particularly important for cell delivery. Therefore, the swelling ratio of IH and IH + GR hydrogels were evaluated by immersing the lyophilized hydrogels in phosphate buffer saline (PBS) solution until equilibrium. The calculated swelling ratio of the hydrogels is presented in Fig. 5. All hydrogels absorbed large amounts of water, reaching the maximum absorption within two to three days, and maintaining their structural integrity for at least 5 days. This initial swelling might be enhanced by the hydrogen bonding between the water molecules and the amino, carboxyl and hydroxyl groups of the polysaccharides and gelatin [64] The hydrogels then began to gradually lose mass, an effect that is more noticeable in the IH hydrogel which collapsed completely within 8 days. The addition of the graphene to the hydrogels substantially improved the stability of the hydrogels, decreasing the degradation rate or even preventing it. Furthermore, it is known that due to its hydrophobic nature, graphene reduces the water uptake of hydrophilic polymers [65]. In this study it can be observed that very low loadings of graphene in the hydrogels slightly decreased the SR. The improved overall hydrogel stability is probably due to the presence of -COOH and -OH groups in

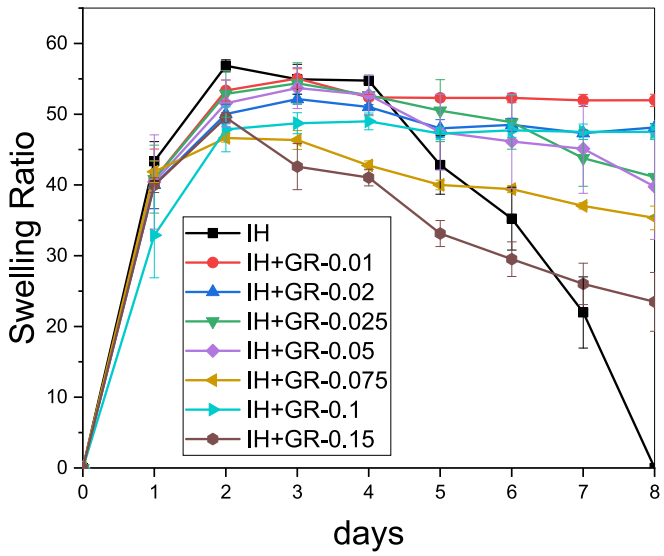

Fig. 5. Swelling ratio of the freeze-dried hydrogels.

graphene nanosheets (<0.1 %), which can also form hydrogen bonds with carrageenans and gelatin, acting as a physical cross-linking point that hinder the swelling of IH + GR hydrogels and improves their physical stability [66]. It is known that -COOH groups are located at the edges of the graphene laminates and Raman data (Fig. 1) support this, as the D′ band is clearly observed. In addition, the graphene-hydrogel hydrogen bonding might interfere in the formation of hydrogen bonding between the hydrogel and water molecules, resulting in a diminution of the swelling ratio of the hydrogels with graphene (Fig. 5). The hydrogel with the least water absorption capacity was the one with the highest graphene concentration (IH + GR-0.15). Despite that, the SR of the graphene containing hydrogels remains relatively high.

3.2.4. Scanning electron microscopy

Fig. 6. shows the morphologies of the freeze-dried hydrogels. The IH hydrogel (Fig. 6A) showed a porous network with three-dimensionally interconnected microstructures due to the combination between gelatin and carrageenan [2,67]. Hydrogels with graphene showed lower pore size than the IH hydrogel (Fig. 6B–H). The pore size seems to decrease with increasing the concentration of graphene, being poorly defined at the highest used graphene concentrations (Fig. 6G–H). The decrease in pore size might be attributed to the extra hydrogen bonding provided by the graphene residual groups to the hydrogel network. It is also in line with the increased stability, slight decrease of swelling capacity and the improved mechanical properties of the graphene hydrogels. Some graphene agglomerations were observed on the hydrogel surfaces, especially at higher graphene concentration.

3.2.5. In vitro biological evaluation

To investigate the biocompatibility of the injectable hydrogels, for the potential applications in tissue repair, cell adhesion and the effect produced by the materials on the cell viability of 3T3-L1 fibroblasts were evaluated by confocal laser microscopy (CLM). We used CLM rather than the methylthiazolyldiphenyl-tetrazolium bromide (MTT) assay, classically used for the evaluation of cellular viability, since in our preliminary assays performed with MTT, graphene caused false positive results (data not shown) [68]. Staining with PI or calcein was performed after 24 h and 48 h of cell contact with the different hydrogels. As shown in Fig. 7, 3T3-L1 cell proliferation in hydrogels containing increasing percentage of graphene was similar to that observed in control gels (without graphene) up to a graphene loading of 0.05 %. However, when graphene reached the concentration of 0.075 %, cell proliferation decreased (Fig. 7d and h). The control hydrogel (without graphene) was previously reported to be biocompatible and to promote the proliferation of the 3T3-L1 cells. It enhanced the cellular adhesion and improved the spreading of the cells inside the hydrogel matrix. [53]. In all the hydrogels tested so far, 3T3-L1 cells were able to proliferate inside the gel structure and showed higher spreading after 48 h (Fig. 7e–h), which is a morphological visual indicator of an appropriate cell attachment.

As shown in Fig. 8a, quantification of the cell number (expressed as n° of cells /mm^2) after 48 h suggested a clear detrimental effect of graphene on cell proliferation at the highest concentration tested so far. The addition of graphene at a concentration up to 0.05 % w/v did not significantly affect the cell count inside the hydrogels (Fig. 8a). The count of the 3T3-L1 cells in the hydrogels with higher graphene concentrations (0.075 % w/v) was significantly lower which indicates certain interference with the proliferation rate of the cells. Despite that,

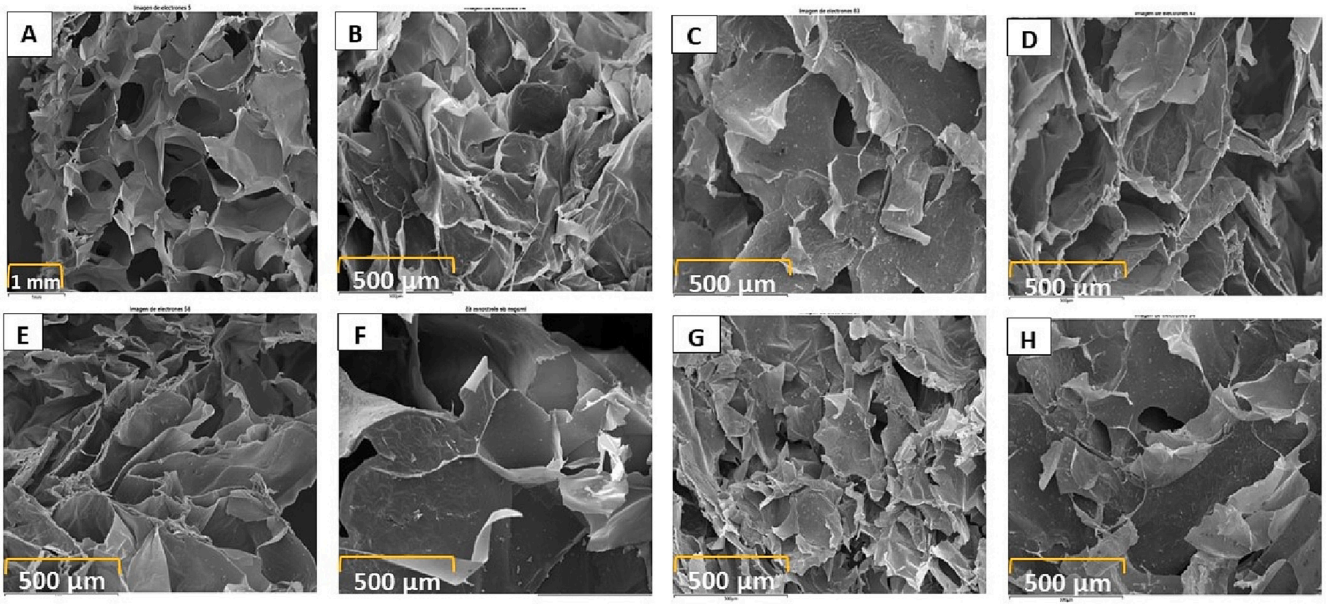

Fig. 6. SEM images of the hydrogels: IH (A); IH + GR-0.01 (B); IH + GR-0.02 (C); IH + GR-0.025 (D); IH + GR-0.05 (E); IH + GR-0.075 (F); IH + GR-0.1 (G); and IH + GR-0.15 (H).

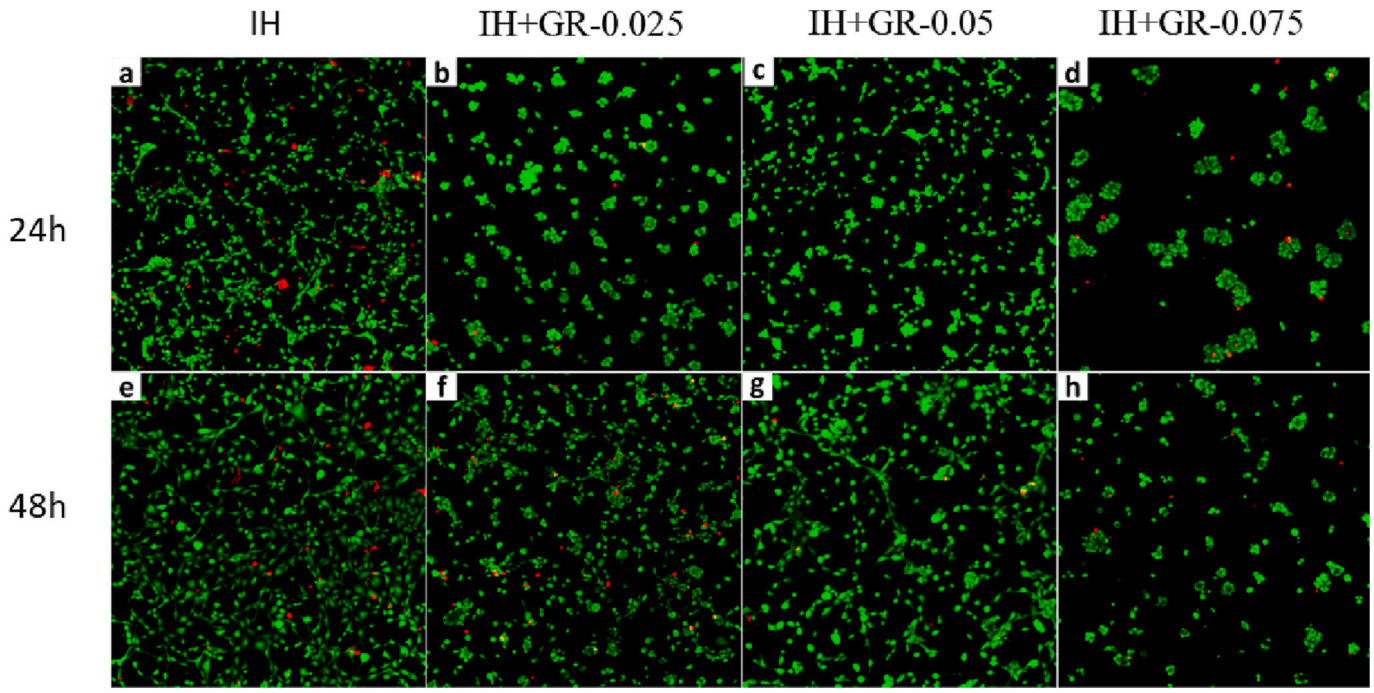

Fig. 7. Confocal laser microscopy images obtained after 24 h (a–d) and 48 h (e–h) showing the live/dead staining of 3T3-L1 fibroblasts cultured with the hydrogels IH (a, e), IH + GR-0.025 (b, f), IH + GR-0.05 (c, g) and IH + GR-0.075 (d, h).

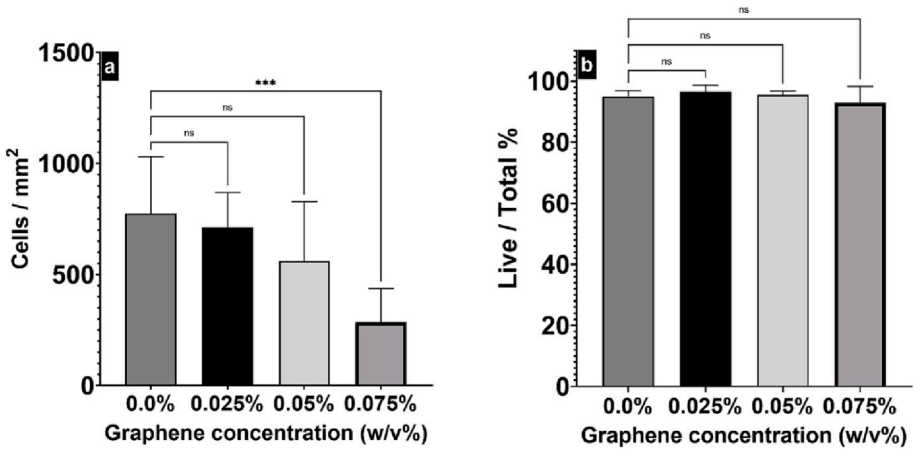

Fig. 8. Count (a) and the Live/total (b) percentage of the cell proliferated after 48 h inside the hydrogels with different graphene concentrations (ns = non significant, ***P < 0.001).

graphene increasing concentrations in the hydrogels likely did not affect the ratio of live/total cells, counted after 48 h, suggesting that graphene, per se, did not show relevant cytotoxic effects (Fig. 8b).

Taken together, these data point out that the hydrogels having graphene concentrations of 0.025 and 0.05 % w/v, which showed enhanced mechanical and swelling performance, demonstrated also promising clues of biocompatibility. These results are in agreement with other studies that reported the biocompatibility of hybrid material systems containing κ-carrageenan and graphene oxide for targeted doxorubicin delivery and tissue engineering. Graphene and graphene oxide have been studied for wide variety of diagnostic, therapeutic and tissue engineering applications, however, the discussion about their possible cytotoxicity is still open and widely controversial [69]. Many studies have reported the biocompatibility of graphene and different graphene containing biomaterials [70–72]. On the other hand, Duan et al. demonstrated both experimentally and by simulation the cytotoxicity of graphene through pore formation on the cell membrane [73]. Liao et al. described graphene and graphene oxide to have haemolytic effect on red blood cells [68]. Interestingly, the same study reported that this haemolytic effect was eliminated when the graphene was coated with chitosan. Embedding the graphene within a biocompatible polymeric matrix seemed to decrease a possible cytotoxic effect of the nanosheets. In addition, the physical interactions between the graphene and the polymeric chains may lead eventually to hindering the mobility of these nanosheets, thus decreasing their contact with the surface of the cells. Collectively, the biocompatibility of graphene and graphene containing biomaterial seems to be dependent on diverse factors including the morphology, size, functional groups, purity, and the degree of aggregation of the graphene nanosheets, in addition to the interactions with the surrounding biomaterials.

4. Conclusions

The injectable hybrid hydrogels based on carrageenan/locust bean

gum/gelatin reinforced by green graphene were prepared using a physical crosslinking strategy. The well-dispersed green graphene and the multiple physical bonds in hydrogels are keys for its injectability, stability in physiological buffered salt solution as well as a good mechanical performance. The hybrid hydrogels possessed porous structure with water uptake ability, which favours living cells ingrowth. The injectable hybrid hydrogels with graphene content between 0.02 and 0.05 % w/v not only enhanced mechanical property but also promoted the viability, cell attachment, and proliferation, exhibiting future promising for application in regenerative medicine. Additional in vivo analysis would strengthen the proposed application of these hydrogels.

CRediT authorship contribution statement

All persons who meet authorship criteria are listed as authors, and all authors certify that they have participated sufficiently in the work to take public responsibility for the content, including participation in the concept, design, analysis, writing, or revision of the manuscript.

Declaration of competing interest

The authors declare that they have no known competing financial interests or personal relationships that could have appeared to influence the work reported in this paper.

Acknowledgement

The research leading to these results received funding from the Xunta de Galicia Government: program of consolidation and structuring competitive research units [grant number: ED431C 2019/17]. Y.F. is a 'Sara Borrell' researcher funded by Instituto de Salud Carlos III (ISCIII) and co-funded by Fondo Europeo de Desarrollo Regional (FEDER) [CD21/00042]. Thanks to Corfo 22CVID-206836, CIPA, ANID Regional, GORE BIO BIO, R17A10003, ACE210016, ACE210012. Funding for open access charge was provided by Universidade da Coruña/CISUG.

References

[1] D.P. Pacheco, L. Zorzetto, P. Petrini, Soft tissue application of biocomposites, in: Biomedical Composites, Elsevier, 2017, pp. 59–82, https://doi.org/10.1016/b978-0-08-100752-5.00004-4.
[2] N. Pettinelli, S. Rodríguez-Llamazares, R. Bouza, L. Barral, S. Feijoo-Bandín, F. Lago, Carrageenan-based physically crosslinked injectable hydrogel for wound healing and tissue repairing applications, Int. J. Pharm. 589 (2020), https://doi.org/10.1016/j.ijpharm.2020.119828.
[3] F.A. Ngwabebhoh, R. Patwa, O. Zandraa, N. Saha, P. Saha, Preparation and characterization of injectable self-antibacterial gelatin/carrageenan/bacterial cellulose hydrogel scaffolds for wound healing application, J. Drug Deliv. Sci. Technol. 63 (2021), https://doi.org/10.1016/j.jddst.2021.102415.
[4] D.A. Gyles, L.D. Castro, J.O.C. Silva, R.M. Ribeiro-Costa, A review of the designs and prominent biomedical advances of natural and synthetic hydrogel formulations, Eur. Polym. J. 88 (2017) 373–392, https://doi.org/10.1016/j.eurpolymj.2017.01.027.
[5] N. Pettinelli, S. Rodríguez-Llamazares, V. Abella, L. Barral, R. Bouza, Y. Farrag, F. Lago, Entrapment of chitosan, pectin or κ-carrageenan within methacrylate based hydrogels: effect on swelling and mechanical properties, Mater. Sci. Eng. C 96 (2019) 583–590, https://doi.org/10.1016/j.msec.2018.11.071.
[6] Z. Fan, P. Cheng, Y. Gao, D. Wang, G. Jia, P. Zhang, S. Prakash, Z. Wang, J. Han, Understanding the rheological properties of a novel composite salecan/gellan hydrogels, Food Hydrocoll. 123 (2022), https://doi.org/10.1016/j.foodhyd.2021.107162.
[7] T. Su, W. Zhao, L. Wu, W. Dong, X. Qi, Facile fabrication of functional hydrogels consisting of pullulan and polydopamine fibers for drug delivery, Int. J. Biol. Macromol. 163 (2020) 366–374, https://doi.org/10.1016/J.IJBIOMAC.2020.06.283.
[8] W. Wei, X. Qi, J. Li, Y. Zhong, G. Zuo, X. Pan, T. Su, J. Zhang, W. Dong, Synthesis and characterization of a novel cationic hydrogel base on salecan-g-PMAPTAC, Int. J. Biol. Macromol. 101 (2017) 474–480, https://doi.org/10.1016/J.IJBIOMAC.2017.03.106.
[9] E.M. Ahmed, Hydrogel: preparation, characterization, and applications: a review, J. Adv. Res. 6 (2015) 105–121, https://doi.org/10.1016/j.jare.2013.07.006.
[10] N. Zoratto, P. Matricardi, Semi-IPNs and IPN-based hydrogels, in: Polymeric Gels, Elsevier, 2018, pp. 91–124, https://doi.org/10.1016/b978-0-08-102179-8.00004-1.
[11] T. Funami, M. Hiroe, S. Noda, I. Asai, S. Ikeda, K. Nishinari, Influence of molecular structure imaged with atomic force microscopy on the rheological behavior of carrageenan aqueous systems in the presence or absence of cations, Food Hydrocoll. 21 (2007) 617–629, https://doi.org/10.1016/j.foodhyd.2006.07.013.
[12] S. Ramakrishnan, R.K. Prud'Homme, Behavior of κ-carrageenan in glycerol and sorbitol solutions, Carbohydr. Polym. 43 (2000) 327–332, https://doi.org/10.1016/S0144-8617(00)00177-6.
[13] N.A. Peppas, A.S. Hoffman, Hydrogels, Biomater. Sci. (2020) 153–166, https://doi.org/10.1016/B978-0-12-816137-1.00014-3.
[14] H.F. Darge, A.T. Andrgie, H.C. Tsai, J.Y. Lai, Polysaccharide and polypeptide based injectable thermo-sensitive hydrogels for local biomedical applications, Int. J. Biol. Macromol. 133 (2019) 545–563, https://doi.org/10.1016/j.ijbiomac.2019.04.131.
[15] Y. Luo, L. Fan, C. Liu, H. Wen, S. Wang, P. Guan, D. Chen, C. Ning, L. Zhou, G. Tan, An injectable, self-healing, electroconductive extracellular matrix-based hydrogel for enhancing tissue repair after traumatic spinal cord injury, Bioact Mater. 7 (2022) 98–111, https://doi.org/10.1016/j.bioactmat.2021.05.039.
[16] B. Qian, Q. Yang, M. Wang, S. Huang, C. Jiang, H. Shi, Q. Long, M. Zhou, Q. Zhao, X. Ye, Encapsulation of lyophilized platelet-rich fibrin in alginate-hyaluronic acid hydrogel as a novel vascularized substitution for myocardial infarction, Bioact. Mater. 7 (2022) 401–411, https://doi.org/10.1016/j.bioactmat.2021.05.042.
[17] X. Jiang, X. Yang, B. Yang, L. Zhang, A. Lu, Highly self-healable and injectable cellulose hydrogels via rapid hydrazone linkage for drug delivery and 3D cell culture, Carbohydr. Polym. 273 (2021), https://doi.org/10.1016/j.carbpol.2021.118547.
[18] X. Qi, T. Su, M. Zhang, X. Tong, W. Pan, Q. Zeng, J. Shen, Sustainable, flexible and biocompatible hydrogels derived from microbial polysaccharides with tailorable structures for tissue engineering, Carbohydr. Polym. 237 (2020), 116160, https://doi.org/10.1016/J.CARBPOL.2020.116160.
[19] X. Qi, M. Zhang, T. Su, W. Pan, X. Tong, Q. Zeng, W. Xiong, N. Jiang, Y. Qian, Z. Li, X. He, L. Shen, Z. Zhou, J. Shen, Biocompatible hydrogels based on food gums with tunable physicochemical properties as scaffolds for cell culture, J. Agric. Food Chem. 68 (2020) 3770–3778, https://doi.org/10.1021/ACS.JAFC.9B06120/ASSET/IMAGES/LARGE/JF9B06120_0007.JPEG.
[20] A.C. Hernández-González, L. Téllez-Jurado, L.M. Rodríguez-Lorenzo, Alginate hydrogels for bone tissue engineering, from injectables to bioprinting: a review, Carbohydr. Polym. 229 (2020), https://doi.org/10.1016/j.carbpol.2019.115514.
[21] L. Yu, J. Ding, Injectable hydrogels as unique biomedical materials, Chem. Soc. Rev. 37 (2008) 1473–1481, https://doi.org/10.1039/b713009k.
[22] B. Velasco- Rodriguez, T. Diaz-vidal, L.C. Rosales-rivera, C.A. García-González, C. Alvarez-lorenzo, A. Al-modlej, V. Domínguez-arca, G. Prieto, S. Barbosa, J.F. A. Soltero Martínez, P. Taboada, Hybrid methacrylated gelatin and hyaluronic acid hydrogel scaffolds. Preparation and systematic characterization for prospective tissue engineering applications, Int. J. Mol. Sci. 22 (2021) 1–26, https://doi.org/10.3390/ijms22136758.
[23] G.T. İlhan, G. Irmak, M. Gümüşderelioğlu, Microwave assisted methacrylation of kappa carrageenan: a bioink for cartilage tissue engineering, Int. J. Biol. Macromol. 164 (2020) 3523–3534, https://doi.org/10.1016/j.ijbiomac.2020.08.241.
[24] C. Pascual-Garrido, F. Rodriguez-Fontan, E.A. Aisenbrey, K.A. Payne, J. Chahla, L. R. Goodrich, S.J. Bryant, Current and novel injectable hydrogels to treat focal chondral lesions: properties and applicability, J. Orthop. Res. 36 (2018) 64–75, https://doi.org/10.1002/jor.23760.
[25] J. Guan, L. Li, S. Mao, Applications of carrageenan in advanced drug delivery, in: Seaweed Polysaccharides: Isolation, Biological and Biomedical Applications, Elsevier, 2017, pp. 283–303, https://doi.org/10.1016/B978-0-12-809816-5.00015-3.
[26] V.I. Evageliou, P.M. Ryan, E.R. Morris, Effect of monovalent cations on calcium-induced assemblies of kappa carrageenan, Food Hydrocoll. 86 (2019) 141–145, https://doi.org/10.1016/j.foodhyd.2018.03.018.
[27] S. Graham, P.F. Marina, A. Blencowe, Thermoresponsive polysaccharides and their thermoreversible physical hydrogel networks, Carbohydr. Polym. 207 (2019) 143–159, https://doi.org/10.1016/j.carbpol.2018.11.053.
[28] J. Necas, L. Bartosikova, Carrageenan: a review, Vet. Med. (Praha) 58 (2013) 187–205, https://doi.org/10.17221/6758-VETMED.
[29] V.L. Campo, D.F. Kawano, D.B. da Silva, I. Carvalho, Carrageenans: biological properties, chemical modifications and structural analysis - a review, Carbohydr. Polym. 77 (2009) 167–180, https://doi.org/10.1016/j.carbpol.2009.01.020.
[30] Y. Cao, S. Li, Y. Fang, K. Nishinari, G.O. Phillips, A. Lerbret, A. Assifaoui, Specific binding of trivalent metal ions to λ-carrageenan, Int. J. Biol. Macromol. 109 (2018) 350–356, https://doi.org/10.1016/j.ijbiomac.2017.12.095.
[31] C.A. Running, R. Falshaw, S. Janaswamy, Trivalent iron induced gelation in lambda-carrageenan, Carbohydr. Polym. 87 (2012) 2735–2739, https://doi.org/10.1016/j.carbpol.2011.11.018.
[32] R. Yegappan, V. Selvaprithiviraj, S. Amirthalingam, R. Jayakumar, Carrageenan based hydrogels for drug delivery, tissue engineering and wound healing, Carbohydr. Polym. 198 (2018) 385–400, https://doi.org/10.1016/j.carbpol.2018.06.086.
[33] A. Aldalbahi, J. Chu, P. Feng, M. in het Panhuis, Conducting composite materials from the biopolymer kappa-carrageenan and carbon nanotubes, Beilstein J. Nanotechnol. 3 (2012) 415–427, https://doi.org/10.3762/bjnano.3.48.
[34] F. van de Velde, Structure and function of hybrid carrageenans, Food Hydrocoll. 22 (2008) 727–734, https://doi.org/10.1016/j.foodhyd.2007.05.013.
[35] F. van de Velde, H.A. Peppelman, H.S. Rollema, R.H. Tromp, On the structure of κ/ι-hybrid carrageenans, Carbohydr. Res. 331 (2001) 271–283, https://doi.org/10.1016/S0008-6215(01)00054-4.

[36] V.T.N.T. Bui, B.T. Nguyen, T. Nicolai, F. Renou, Mixed iota and kappa carrageenan gels in the presence of both calcium and potassium ions, Carbohydr. Polym. 223 (2019), https://doi.org/10.1016/j.carbpol.2019.115107.
[37] Y. Zhu, S. Murali, W. Cai, X. Li, J.W. Suk, J.R. Potts, R.S. Ruoff, Graphene and graphene oxide: synthesis, properties, and applications, Adv. Mater. 22 (2010) 3906–3924, https://doi.org/10.1002/ADMA.201001068.
[38] O.C. Compton, S.T. Nguyen, Graphene oxide, highly reduced graphene oxide, and graphene: versatile building blocks for carbon-based materials, Small 6 (2010) 711–723, https://doi.org/10.1002/SMLL.200901934.
[39] A. Kobyliukh, K. Olszowska, M. Godzierz, A. Kordyka, J. Kubacki, Y. Mamunya, S. Pusz, I. Stoycheva, U. Szeluga, Effect of graphene material structure and iron oxides deposition method on morphology and properties of graphene/iron oxide hybrids, Appl. Surf. Sci. 573 (2022), https://doi.org/10.1016/j.apsusc.2021.151567.
[40] J. Phiri, P. Gane, T.C. Maloney, General overview of graphene: production, properties and application in polymer composites, Mater. Sci. Eng. B Solid State Mater. Adv. Technol. 215 (2017) 9–28, https://doi.org/10.1016/j.mseb.2016.10.004.
[41] A.T. Smith, A.M. LaChance, S. Zeng, B. Liu, L. Sun, Synthesis, properties, and applications of graphene oxide/reduced graphene oxide and their nanocomposites, NanoMater. Sci. 1 (2019) 31–47, https://doi.org/10.1016/j.nanoms.2019.02.004.
[42] M. Kim, C. Lee, J. Jang, Fabrication of highly flexible, scalable, and high-performance supercapacitors using polyaniline/reduced graphene oxide film with enhanced electrical conductivity and crystallinity, Adv. Funct. Mater. 24 (2014) 2489–2499, https://doi.org/10.1002/adfm.201303282.
[43] A. Paul, A. Hasan, H. al Kindi, A.K. Gaharwar, V.T.S. Rao, M. Nikkhah, S.R. Shin, D. Krafft, M.R. Dokmeci, D. Shum-Tim, A. Khademhosseini, Injectable graphene oxide/hydrogel-based angiogenic gene delivery system for vasculogenesis and cardiac repair, ACS Nano 8 (2014) 8050–8062, https://doi.org/10.1021/nn5020787.
[44] C. Chung, Y.K. Kim, D. Shin, S.R. Ryoo, B.H. Hong, D.H. Min, Biomedical applications of graphene and graphene oxide, Acc. Chem. Res. 46 (2013) 2211–2224, https://doi.org/10.1021/ar300159f.
[45] S.R. Shin, B. Aghaei-Ghareh-Bolagh, X. Gao, M. Nikkhah, S.M. Jung, A. Dolatshahi-Pirouz, S.B. Kim, S.M. Kim, M.R. Dokmeci, X. Tang, A. Khademhosseini, Layer-by-layer assembly of 3D tissue constructs with functionalized graphene, Adv. Funct. Mater. 24 (2014) 6136–6144, https://doi.org/10.1002/adfm.201401300.
[46] K. Vinothini, N.K. Rajendran, M.A. Munusamy, A.A. Alarfaj, M. Rajan, Development of biotin molecule targeted cancer cell drug delivery of doxorubicin loaded κ-carrageenan grafted graphene oxide nanocarrier, Mater. Sci. Eng. C 100 (2019) 676–687, https://doi.org/10.1016/j.msec.2019.03.011.
[47] H. Mokhtari, M. Kharaziha, F. Karimzadeh, S. Tavakoli, An injectable mechanically robust hydrogel of kappa-carrageenan-dopamine functionalized graphene oxide for promoting cell growth, Carbohydr. Polym. 214 (2019) 234–249, https://doi.org/10.1016/j.carbpol.2019.03.030.
[48] M.U. Aslam Khan, M.A. Raza, H. Mehboob, M.R. Abdul Kadir, S.I. Abd Razak, S. A. Shah, M.Z. Iqbal, R. Amin, Development and: in vitro evaluation of κ-carrageenan based polymeric hybrid nanocomposite scaffolds for bone tissue engineering, RSC Adv. 10 (2020) 40529–40542, https://doi.org/10.1039/d0ra07446b.
[49] H. Liu, J. Cheng, F. Chen, F. Hou, D. Bai, P. Xi, Z. Zeng, Biomimetic and cell-mediated mineralization of hydroxyapatite by carrageenan functionalized graphene oxide, ACS Appl. Mater. Interfaces 6 (2014) 3132–3140, https://doi.org/10.1021/am4057826.
[50] L.F. Santos, I.J. Correia, A.S. Silva, J.F. Mano, Biomaterials for drug delivery patches, Eur. J. Pharm. Sci. 118 (2018) 49–66, https://doi.org/10.1016/J.EJPS.2018.03.020.
[51] A.C. Pinheiro, A.I. Bourbon, C. Rocha, C. Ribeiro, J.M. Maia, M.P. Gonalves, J. A. Teixeira, A.A. Vicente, Rheological characterization of κ-carrageenan/galactomannan and xanthan/galactomannan gels: comparison of galactomannans from non-traditional sources with conventional galactomannans, Carbohydr. Polym. 83 (2011) 392–399, https://doi.org/10.1016/J.CARBPOL.2010.07.058.
[52] L. Tytgat, M. Vagenende, H. Declercq, J.C. Martins, H. Thienpont, H. Ottevaere, P. Dubruel, S. van Vlierberghe, Synergistic effect of κ-carrageenan and gelatin blends towards adipose tissue engineering, Carbohydr. Polym. 189 (2018) 1–9, https://doi.org/10.1016/J.CARBPOL.2018.02.002.
[53] N. Pettinelli, S. Rodríguez-Llamazares, R. Bouza, L. Barral, S. Feijoo-Bandín, F. Lago, Carrageenan-based physically crosslinked injectable hydrogel for wound healing and tissue repairing applications, Int. J. Pharm. 589 (2020), 119828, https://doi.org/10.1016/j.ijpharm.2020.119828.
[54] E.J. Lee, E. Kang, S.W. Kang, K.M. Huh, Thermo-irreversible glycol chitosan/hyaluronic acid blend hydrogel for injectable tissue engineering, Carbohydr. Polym. 244 (2020), 116432, https://doi.org/10.1016/J.CARBPOL.2020.116432.
[55] J. Wang, Z. Chen, B. Chen, Adsorption of polycyclic aromatic hydrocarbons by graphene and graphene oxide nanosheets, Environ. Sci. Technol. 48 (2014) 4817–4825, https://doi.org/10.1021/ES405227U/SUPPL_FILE/ES405227U_SI_001.PDF.
[56] L.M. Malard, M.A. Pimenta, G. Dresselhaus, M.S. Dresselhaus, Raman spectroscopy in graphene, Phys. Rep. 473 (2009) 51–87, https://doi.org/10.1016/j.physrep.2009.02.003.
[57] S. Eigler, F. Hof, M. Enzelberger-Heim, S. Grimm, P. Müller, A. Hirsch, Statistical Raman microscopy and atomic force microscopy on heterogeneous graphene obtained after reduction of graphene oxide, J. Phys. Chem. C 118 (2014) 7698–7704, https://doi.org/10.1021/JP500580G/SUPPL_FILE/JP500580G_SI_001.PDF.
[58] Y. Hernandez, V. Nicolosi, M. Lotya, F.M. Blighe, Z. Sun, S. De, I.T. McGovern, B. Holland, M. Byrne, Y.K. Gun'ko, J.J. Boland, P. Niraj, G. Duesberg, S. Krishnamurthy, R. Goodhue, J. Hutchison, V. Scardaci, A.C. Ferrari, J. N. Coleman, High-yield production of graphene by liquid-phase exfoliation of graphite, Nat. Nanotechnol. 3 (2008) 563–568, https://doi.org/10.1038/NNANO.2008.215.
[59] H.J. Salavagione, P.S. Shuttleworth, J.P. Fernández-Blázquez, G.J. Ellis, M. A. Gómez-Fatou, Scalable graphene-based nanocomposite coatings for flexible and washable conductive textiles, Carbon N Y. 167 (2020) 495–503, https://doi.org/10.1016/J.CARBON.2020.05.108.
[60] S. Ganguly, P. Das, P.P. Maity, S. Mondal, S. Ghosh, S. Dhara, N.C. Das, Green reduced graphene oxide toughened semi-IPN monolith hydrogel as dual responsive drug release system: rheological, physicomechanical, and electrical evaluations, J. Phys. Chem. B 122 (2018) 7201–7218, https://doi.org/10.1021/acs.jpcb.8b02919.
[61] Y. Huang, M. Zeng, J. Chen, Y. Wang, Q. Xu, Multi-structural network design and mechanical properties of graphene oxide filled chitosan-based hydrogel nanocomposites, Mater. Des. 148 (2018) 104–114, https://doi.org/10.1016/J.MATDES.2018.03.055.
[62] H. Qin, J. Wang, T. Wang, X. Gao, Q. Wan, X. Pei, Preparation and characterization of chitosan/β-glycerophosphate thermal-sensitive hydrogel reinforced by graphene oxide, Front. Chem. 6 (2018) 565, https://doi.org/10.3389/FCHEM.2018.00565/BIBTEX.
[63] H. Zhang, X. Wu, Z. Qin, X. Sun, H. Zhang, Q. Yu, M. Yao, S. He, X. Dong, F. Yao, J. Li, Dual physically cross-linked carboxymethyl cellulose-based hydrogel with high stretchability and toughness as sensitive strain sensors, Cellulose 27 (2020) 9975–9989, https://doi.org/10.1007/S10570-020-03463-5/FIGURES/7.
[64] J. Li, B. Yang, Y. Qian, Q. Wang, R. Han, T. Hao, Y. Shu, Y. Zhang, F. Yao, C. Wang, Iota-carrageenan/chitosan/gelatin scaffold for the osteogenic differentiation of adipose-derived MSCs in vitro, J. Biomed. Mater. Res. B Appl. Biomater. 103 (2015) 1498–1510, https://doi.org/10.1002/JBM.B.33339/FORMAT/PDF.
[65] A. Flores, H.J. Salavagione, F. Ania, G. Martínez, G. Ellis, M.A. Gómez-Fatou, The overlooked role of reduced graphene oxide in the reinforcement of hydrophilic polymers, J. Mater. Chem. C Mater. 3 (2015) 1177–1180, https://doi.org/10.1039/C4TC02425G.
[66] L. Zhang, Z. Wang, C. Xu, Y. Li, J. Gao, W. Wang, Y. Liu, High strength graphene oxide/polyvinyl alcohol composite hydrogels, J. Mater. Chem. 21 (2011) 10399–10406, https://doi.org/10.1039/C0JM04043F.
[67] J.S. Varghese, N. Chellappa, N.N. Fathima, Gelatin-carrageenan hydrogels: role of pore size distribution on drug delivery process, Colloids Surf. B Biointerfaces 113 (2014) 346–351, https://doi.org/10.1016/J.COLSURFB.2013.08.049.
[68] K. Liao, Y. Lin, C.W. Macosko, C.L. Haynes, Cytotoxicity of graphene oxide and graphene in human erythrocytes and skin fibroblasts, ACS Appl. Mater. Interfaces 3 (2011) 2607–2615, https://doi.org/10.1021/am200428v.
[69] J. Li, H. Zeng, Z. Zeng, Y. Zeng, T. Xie, Promising graphene-based nanomaterials and their biomedical applications and potential risks: a comprehensive review, ACS Biomater. Sci. Eng. 7 (2021) 5363–5396, https://doi.org/10.1021/acsbiomaterials.1c00875.
[70] I. Lasocka, L. Szulc-Dąbrowska, M. Skibniewski, E. Skibniewska, K. Gregorczyk-Zboroch, I. Pasternak, M.H. Kalbacova, Cytocompatibility of graphene monolayer and its impact on focal cell adhesion, mitochondrial morphology and activity in balb/3t3 fibroblasts, Materials. 14 (2021) 1–16, https://doi.org/10.3390/ma14030643.
[71] W. Hanif, A. Hardiansyah, A. Randy, L.A.T.W. Asri, Physically crosslinked PVA/graphene-based materials/aloe vera hydrogel with antibacterial activity, RSC Adv. 11 (2021) 29029–29041, https://doi.org/10.1039/d1ra04992e.
[72] J. Park, P. Kravchuk, A. Krishnaprasad, T. Roy, E.H. Kang, Graphene enhances actin filament assembly kinetics and modulates NIH-3T3 fibroblast cell spreading, Int. J. Mol. Sci. 23 (2022) 509, https://doi.org/10.3390/IJMS23010509/S1.
[73] G. Duan, Y. Zhang, B. Luan, J.K. Weber, R.W.R. Zhou, Z. Yang, L. Zhao, J. Xu, J. Luo, R.W.R. Zhou, Graphene-induced pore formation on cell membranes, Sci. Rep. 7 (2017) 1–12, https://doi.org/10.1038/srep42767.